CO-REGISTRATION OF PHOTOGRAMMETRIC AND LIDAR DATA: METHODOLOGY AND CASE STUDY

Ayman Habib[1], Mwafag Ghanma[1], Edson Mitishita[2]

[1]Department of Geomatics Engineering
University of Calgary
2500 University Drive NW
Calgary, Alberta, T2N 1N4, Canada
Tel: (403) 220-7105; Fax: (403) 284-1980
Email: habib@geomatics.ucalgary.ca

[2]Setor de Ciências da Terra - Departamento de Geomática
Universidade Federal do Paraná
Caixa Postal 19.001
81.531-970 Curitiba, Paraná, Brasil
Tel: 55 41 361-3161/361-3164 - Fax 55 41 361-3161
Email: mitishita@ufpr.br

ABSTRACT

Registration activities combine data from different sources in order to attain higher accuracy and derive more information than available from one source. The increasing availability of a wide variety of sensors capable of capturing high quality and complementary data requires parallel efforts for developing accurate and robust registration techniques. Currently, photogrammetric and LIDAR systems are being incorporated in a wide spectrum of mapping applications such as city modeling, surface reconstruction, and object recognition. Photogrammetric processing of overlapping imagery provides accurate information regarding object space break-lines in addition to an explicit semantic description of the photographed objects. On the other hand, LIDAR systems supply dense geometric surface information in the form of non-selective points. Considering the properties of photogrammetric and LIDAR data, it is clear that the two technologies provide complementary information. However, the synergic characteristics of both systems can be fully utilized only after successful registration of the photogrammetric and LIDAR data relative to a common reference frame. The registration methodology has to deal with three issues: registration primitives, transformation function, and similarity measure. This paper presents two methodologies for utilizing straight-line features derived from both datasets as the registration primitives. The first methodology directly incorporates the LIDAR lines as control information in the photogrammetric triangulation. The second methodology starts by generating a photogrammetric model relative to an arbitrary datum. Then, LIDAR features are used as control information for the absolute orientation of the photogrammetric model. In addition to the registration methodologies, the paper presents a comparative analysis between two approaches for extracting linear features from raw and processed/interpolated LIDAR data. Also, a comparative analysis between metric analog and amateur digital cameras within the registration process will be presented. The performance analysis is based on the quality of fit of the final alignment between the LIDAR and photogrammetric models.

Keywords: Registration, LIDAR, photogrammetry, triangulation, linear features, absolute orientation.

1. INTRODUCTION

Traditional mapping procedures have gone through major developments due to significant improvements in the underlying hardware and software systems as well as newly emerging data collection techniques such as high quality digital imaging and LIDAR systems. The increasing volume and diverse characteristics of the collected data call for the development of efficient and reliable co-registration procedures. This need is motivated by the growing demand for accurate information pertaining to physical surfaces for a variety of applications (e.g., automatic DEM generation, city modeling, and object recognition). In this regard, LIDAR and photogrammetric systems are receiving major attention due to their complementary characteristics and potential. LIDAR has been conceived to directly and accurately capture digital surfaces. LIDAR systems are rapidly maturing on the hardware and supporting software levels. Lower price tag and increased accuracy of new LIDAR systems are causing an exponential profusion and availability of LIDAR datasets. An appealing feature of the LIDAR output is the direct acquisition of three dimensional

coordinates of object space points. However, there is no inherent redundancy in reconstructed surfaces from LIDAR systems. Therefore, the quality of the derived information depends on the accuracy and the validity of the calibration parameters of the different components comprising the LIDAR system. Another characteristic of LIDAR surfaces is that they are mainly positional. In other words, it is difficult to derive semantic information regarding the captured surfaces (e.g., material and type of observed structures) (BALTSAVIAS, 1999).

In contrast to LIDAR systems, reconstructed surfaces from photogrammetric measurements possess rich semantic information that can be easily identified in the captured imagery. Moreover, reconstructed surfaces tend to be very accurate due to the inherent redundancy associated with photogrammetric intersection. The drawback of photogrammetric surface reconstruction is the significant time consumed by the process of manually identifying conjugate points in overlapping images (matching problem). On the other hand, automating the matching problem remains to be a difficult and unreliable task especially when dealing with large scale imagery over urban areas (SCHENK and Csatho, 2002). Full utilization of the complementary characteristics of LIDAR and photogrammetric systems can be achieved by the integration of the acquired data. Such integration would lead to a complete surface description. The quality of the integration outcome unquestionably depends on the validity of the calibration parameters associated with each individual system and the accuracy of the co-registration process of the respective data (POSTOLOV et al., 1999).

The majority of registration methodologies rely on point primitives for solving the registration problem between two datasets. Such methodologies are not applicable to LIDAR surfaces since they correspond to laser footprints instead of distinct points that could be identified in the imagery (BALTSAVIAS, 1999). Conventionally, surface-to-surface registration and comparison have been achieved by interpolating both datasets into a uniform grid. The comparison is then reduced to estimating the necessary shifts by analyzing the elevation differences at corresponding grid posts (EBNER and Ohlhof, 1994; KILIAN et al., 1996). This approach has several limitations. First, the interpolation to a grid will introduce errors especially when dealing with captured surfaces over urban areas. Moreover, minimizing the differences between surfaces along the z-direction is only valid when dealing with horizontal planar surfaces (HABIB and Schenk, 1999). POSTOLOV et al. (1999) presented another approach, which works on the original scattered data without prior interpolation. However, the implementation procedure involves an interpolation of one surface at the location of conjugate points on the other surface. Additionally, the registration is based on minimizing the differences between the two surfaces along the z-direction. SCHENK (1999) introduced an alternative approach, where distances between points of one surface along surface normals to locally interpolated patches of the other surface are minimized. HABIB et al. (2001) implemented this methodology within a comprehensive automatic registration procedure. This procedure is based on processing the photogrammetric data to produce object space planar patches. This might not be always possible since photogrammetric surfaces provide accurate information along object space discontinuities while supplying almost no information along homogeneous surfaces with uniform texture.

This paper introduces two approaches for the co-registration of LIDAR and photogrammetric surfaces relative to a common reference frame. The registration is achieved through the use of linear features derived from LIDAR data as control information for aligning the photogrammetric model relative to the LIDAR reference frame. The following section addresses the general methodology and mathematical models of the suggested approaches. In addition, we present different alternatives for the extraction of linear features from the LIDAR data. Section 3 outlines the experimental results from real datasets captured by LIDAR, analog/metric cameras, and digital/amateur cameras. Finally, Section 4 highlights the research conclusions and recommendations for future work.

2. REGISTRATION PROBLEM AND METHODOLOGY

2.1 Introduction

The registration process, in its basic definition, aims at combining multiple datasets acquired by different sensors in order to achieve better accuracy and enhanced inference about the environment than could be attained through the use of a single sensor. In general, a registration methodology must deal with three issues. First, a decision has to be made regarding the choice of primitives for the registration procedure. The second issue is concerned with establishing a registration transformation function that mathematically relates the datasets under consideration. Finally, a similarity measure should be devised to ensure the coincidence of conjugate primitives after applying the appropriate transformation function (BROWN, 1992). The following sub-sections present a brief overview of the basic components of the registration process. Then, various techniques for the co-registration of photogrammetric and LIDAR datasets are presented.

2.2 Registration primitives

To register two datasets, common features have to be identified and extracted. These features will be subsequently used as the registration primitives relating the datasets in question. The chosen primitives greatly influence subsequent registration steps. Hence, it is crucial to decide upon the appropriate primitives to be used for establishing the transformation between the datasets under consideration (HABIB and Schenk,

1999).

In registration problems involving spatial data, the three fundamental and most commonly used registration primitives are points, lines, and areal regions (refer to Figure 1 for examples of such primitives in imagery). Candidate features include road intersections, corners of buildings, rivers, coastlines, roads, lakes, and/or similar dominant man-made or natural structures.

Distinct Points | Linear Features | Areal Regions

Figure 1. - Examples of primitive alternatives in imagery

Traditional procedures for registering two datasets require interactive selection of tie points, which are then used to determine the parameters of a registration transformation function from one dataset reference frame to the other. However, such a procedure is not convenient for registration activities involving LIDAR and image datasets where it is nearly impossible to link the laser footprint with the corresponding image point. However, at a higher processing cost, three intersecting LIDAR patches can be segmented and utilized to extract points, which can be then identified in the imagery. The above facts exclude point primitives from being appropriate registration primitives.

Consequently, linear and areal features are the other potential primitives that can be more suitable for datasets involving LIDAR data. For these primitives, the geometric distribution of individual points makes up the feature rather than individual occurrences, Figure 2. Linear features can be directly measured in overlapping imagery. Conjugate LIDAR lines can be extracted through the use of homogeneous patch segmentation followed by intersection techniques, Figure 3a. Alternatively, LIDAR lines can be directly identified in the intensity images produced by most of today's LIDAR systems, Figure 3b.

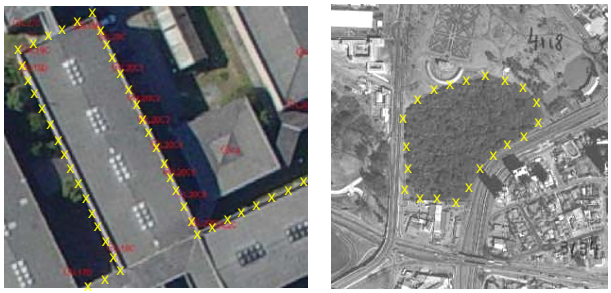

Figure 2. - Line and areas as clusters of individually measured points

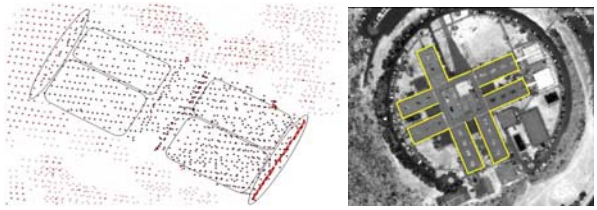

(a) (b)

Figure 3. - LIDAR lines from intersecting planar patches (a) and as measured from intensity image (b)

Areal primitives (e.g., lakes, roofs, and homogeneous regions) can be extracted from LIDAR datasets using classification or segmentation algorithms. However, areal features are not suited for photogrammetric datasets since there are no established procedures for deriving object space areal features from corresponding features in the image space. Therefore, linear features are more appropriate than areal features due to their abundant availability in nature and the simplicity of the extraction algorithms. Moreover, the utilization of linear features allows for the consideration of areal features, which can be represented as a sequence of linear features along their boundaries. In conclusion, linear features are considered to be the best primitives for the following reasons:

- Compared to distinct points, linear features have higher semantics, which can be useful for subsequent processes (such as DEM generation, map compilation, change detection, and object recognition).
- It is easier to automatically extract linear features from different-type and different-resolution datasets rather than distinct points. This can be ascribed to the nature of linear features, since they represent discontinuities in one direction. On the other hand, point features represent discontinuity in all directions.
- Datasets over man-made environments are rich with linear features.
- Linear features can be extracted with adequate accuracy across the direction of the edge.
- Linear features allow for the incorporation of areal features through the use of their boundaries.

Linear features can be represented either by an analytical function (e.g., straight lines, conic sections, or parametric functions) or by a free form shape (HABIB et al., 2002a). In this research, straight-line segments have been chosen as the registration primitives for the following reasons:

- Man-made environments are rich with straight lines.
- Straight lines are easier to detect in different datasets, and the correspondence problem between conjugate features becomes easier to solve.
- Straight-line parameters can be accurately derived from the involved datasets.
- It is straightforward to develop mathematical constraints (similarity measures) describing the correspondence of conjugate straight-line segments.
- Free-form linear features can be represented with sufficient accuracy as a sequence of straight-line segments (polylines).

After selecting straight-line segments as the registration primitives, one must decide on the representation and extraction methodologies from LIDAR and photogrammetric datasets. These issues will be discussed in the following subsections.

2.2.1 Photogrammetric primitives

The representation scheme of straight lines in the object and image space is central to the methodology for producing such features from photogrammetric datasets. Representing object space straight lines using two points along the line is the most convenient representation from a photogrammetric point of view since it yields well-defined line segments (HABIB et al., 2002b). On the other hand, image space lines will be represented by a sequence of 2-D coordinates of intermediate points along the feature. This is an appealing representation since it can handle image space linear features in the presence of distortions as they will cause deviations from straightness. Furthermore, it will allow for the inclusion of linear features in scenes captured by line cameras since the imaging process of such cameras leads to deviations from straightness in image space linear features, which correspond to object space straight lines (HABIB et al., 2002b).

Having settled the representation issue, we now proceed by outlining the methodology of incorporating tie linear features in photogrammetric triangulation. Manipulating tie straight lines, which appear in a group of overlapping images, starts with identifying two end points in one, Figure 4a, or two images, Figure 4b, along the line under consideration. These points will be used to define the corresponding object space line segment. It is worth mentioning that these points need not be identifiable or even visible in other images. Intermediate points along the line are measured in all overlapping images. Similar to the end points, the intermediate points need not be conjugate, Figure 4. The relationship between the image coordinates of the line end points $\{(x_{1'}, y_{1'}),\ (x_{2'}, y_{2'})\}$ and the corresponding ground coordinates $\{(X_1, Y_1, Z_1), (X_2, Y_2, Z_2)\}$ is established through the collinearity equations. Hence, four equations are written for each line. The intermediate points are included into the adjustment procedure through a mathematical constraint, which states that the vector from the perspective centre to any intermediate image point along the line is contained within the plane defined by the perspective centre of that image and the two points defining the straight line in the object space, Figure 5. For a given intermediate point, *i*, a constraint that indicates the points $\{(X_1, Y_1, Z_1),\ (X_2, Y_2, Z_2),\ (X_O'', Y_O'', Z_O'')$ and $(x_i, y_i, 0)\}$ are coplanar, is introduced and mathematically described by Equation 1.

$$\left(\vec{V}_1 \times \vec{V}_2\right) \bullet \vec{V}_3 = 0 \qquad (1)$$

Where:

$\vec{V}_1$ is the vector connecting the perspective centre to the first end point along the object space line,

$\vec{V}_2$ is the vector connecting the perspective centre to the second end point along the object space line, and

$\vec{V}_3$ is the vector connecting the perspective centre to an intermediate point along the corresponding image line.

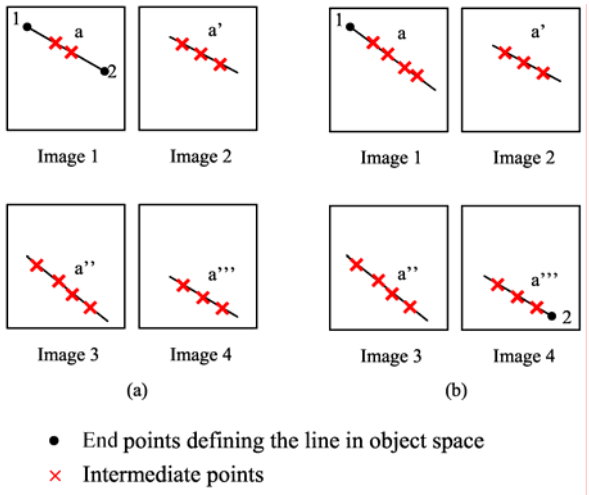

Figure 4. - End points defining the object line are either measured in one image (a) or two images (b)

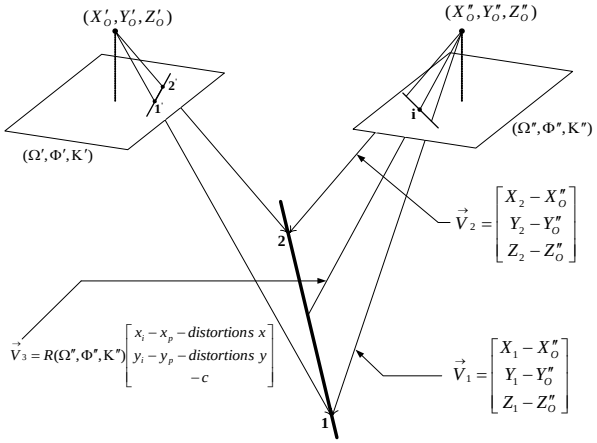

Figure 5. - Perspective transformation between image and object space straight lines and the coplanarity constraint for intermediate points along the line

It is important to note that the three vectors in Equation 1 should be represented relative to a common coordinate system (e.g., the ground coordinate system). The constraint in Equation 1 incorporates the image coordinates of the intermediate point, the Exterior Orientation Parameters (EOP), the Interior Orientation Parameters (IOP) including distortion parameters, as well as the ground coordinates of the points defining the object space line. Such a constraint does not introduce any new parameters and can be written for all intermediate points along the line in overlapping imagery. The number of constraints is equal to the number of intermediate points measured along the

image line.

In some applications, the lines can be used as control features instead of being regular tie lines. In this situation, the object coordinates of line end points are known, hence, these points need not be measured in any of the images. Consequently, image space linear features are represented only by a group of intermediate points measured in all images.

2.2.2 LIDAR primitives

In addition to the derived straight-lines from the photogrammetric model, conjugate LIDAR features have to be extracted to carry out the registration procedure. More explicitly, LIDAR lines will be used as the source of the required control to align the photogrammetric model relative to the LIDAR reference frame. In this regard, one should note that the datum for the LIDAR data is established by the combination of high-quality GPS/INS units onboard the sensor platform.

There are different approaches by which LIDAR lines can be collected. This work presents two alternative approaches. In the first approach, suspected planar patches in the LIDAR dataset are manually identified with the help of corresponding optical imagery, Figures 6 and 7. The selected patches are then checked using a least-squares adjustment to determine whether they are planar or not, and to remove blunders. Finally, neighboring planar patches with different orientation are intersected to determine the end points along object space discontinuities between the patches under consideration.

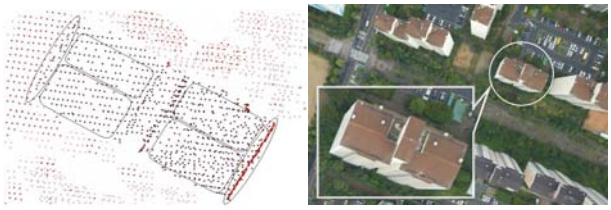

(a) (b)

Figure 6. - Manually identified planar patches in the LIDAR data (a) guided by the corresponding optical image (b) in aerial dataset

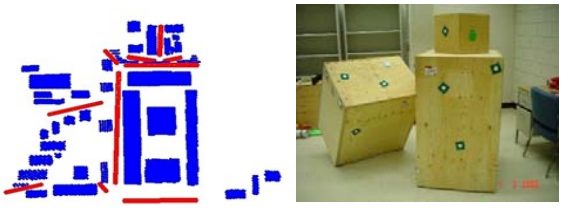

(a) (b)

Figure 7. - Manually identified planar patches in the LIDAR data (a) guided by the corresponding optical image (b) in close-range application

In the second approach, where the goal is to simplify the extraction process, recorded intensity and range data are utilized for direct measurement of linear features. Raw range and intensity data are first interpolated to a uniform grid using the same interpolation method and parameters, producing intensity and range images, Figure 8. Then, photogrammetric linear features are identified on the intensity image from which the planimetric coordinates of line ends are measured while observing height readings from the range image, Figure 8. It is worth mentioning that the interpolation method and applied parameters have a significant effect on the quality of the derived features.

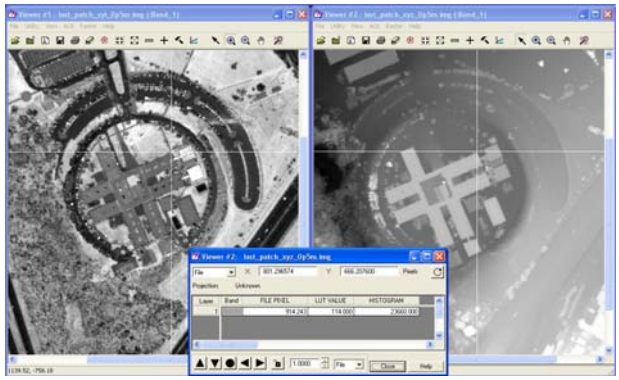

(a) (b)

Figure 8. - Manually measuring planimetric coordinates from the intensity image (a) and height from the range image (b)

Many factors, including the availability of intensity data, play a role in the choice of the extraction method. Automatic extraction of straight lines is beyond the objectives of this study and will be investigated in future work. Following the extraction of straight-lines from both datasets, the focus will be shifted towards selecting a valid and proper transformation function that can faithfully represent the transformation between the involved datasets.

2.3 Transformation Function

The most fundamental problem of any registration technique is the type of spatial transformation or mapping function needed to properly overlay the two datasets. Based on the application scope, a transformation function might be global or local. A global transformation involves a single set of equations which optimally registers the entirety of the involved datasets. On the other hand, local transformation functions utilize several sets of equations by partitioning the area of interest into regions with each one having its own transformation. In general, local transformations are more accurate but also more computationally demanding.

In this study, a global 3-D similarity transformation (conformal transformation) is used, Equation 2, as the registration transformation function. As the name suggests, this type of transformation preserves the geometric similarity where the angles are maintained and distances are changed with the same ratio, the scale

factor. In other words, this transformation defines rigid-body transformation where the true shape is retained. One should note that this transformation assumes that the photogrammetric and LIDAR systems are well calibrated (i.e., there are no systematic errors that have not been compensated for). However, the presence of systematic errors, which cannot be modeled by rigid-body transformation, will manifest itself in a poor quality of fit between the involved datasets following the registration procedure.

$$\begin{bmatrix} X_A \\ Y_A \\ Z_A \end{bmatrix} = \begin{bmatrix} X_T \\ Y_T \\ Z_T \end{bmatrix} + S\ R(\Omega, \Phi, K) \begin{bmatrix} X_a \\ Y_a \\ Z_a \end{bmatrix} \qquad (2)$$

where S is a scale factor,

$(X_T\ Y_T\ Z_T)^T$ is the translation vector between the origins of the photogrammetric and LIDAR coordinate systems,

$R(_{\Omega,\Phi,K})$ is the 3-D orthogonal rotation matrix between the two coordinate systems,

$(X_a\ Y_a\ Z_a)^T$ are the photogrammetric coordinates of a given point, and

$(X_A\ Y_A\ Z_A)^T$ are the coordinates of the corresponding LIDAR point relative to the LIDAR reference frame.

2.4 Similarity Measure

The role of the similarity measure is to introduce the necessary constraints for ensuring the coincidence of conjugate photogrammetric and LIDAR primitives after applying the proper transformation function. The formulation of the similarity measure depends on the selected registration primitives and their respective attributes (i.e., representation scheme). In addition, the similarity measure depends on the utilized methodology for incorporating the LIDAR and photogrammetric data in the registration process. As it has been mentioned earlier, the registration primitives, straight-line segments, will be represented by their end points. One should note that the end points of corresponding photogrammetric and LIDAR lines need not be conjugate. As for the processing methodology, this research will implement two techniques for incorporating the linear features in the registration procedure. The first technique will directly incorporate the LIDAR lines in the photogrammetric bundle adjustment to establish the datum. The other technique is based on preliminary and independent processing of the LIDAR and photogrammetric data. Then, conjugate LIDAR and photogrammetric primitives are utilized in an absolute orientation procedure. The following subsections discuss the involved similarity measures in these processing techniques.

2.4.1 Direct incorporation of LIDAR features in the photogrammetric triangulation

In this approach, LIDAR linear features are used as the source of control in the photogrammetric bundle adjustment (i.e., the LIDAR features will establish the datum for the photogrammetric model). The similarity measure should mathematically ensure that the projected LIDAR lines onto the image space coincide with the corresponding image lines. This is described by the coplanarity constraint expressed in Equation 1. In this processing scenario, the image space features will be represented by a sequence of intermediate points. The end points defining the object space line will not be measured in the imagery since they are already provided by the LIDAR data. One should also note that the 3-D similarity transformation, Equation 2, is implicitly included within the photogrammetric adjustment.

2.4.2 LIDAR features for the absolute orientation of an arbitrarily established photogrammetric model

In this approach, the photogrammetric and LIDAR datasets are separately processed to generate the linear features as follows: First, the photogrammetric data is incorporated in a bundle adjustment procedure, where the datum is established by choosing an arbitrary reference frame. For example, seven of the nine coordinates of three well-distributed tie points can be arbitrarily fixed. Second, conjugate linear features are extracted from the LIDAR data using either planar patch intersection or simultaneous manipulation of the interpolated intensity and range images. Third, corresponding LIDAR and photogrammetric lines are used in an absolute orientation procedure to determine the parameters of the 3-D similarity transformation, Equation 2. The absolute orientation procedure will act as the similarity measure, which will ensure the coincidence of conjugate photogrammetric and LIDAR features after applying the transformation function, Figure 9. The absolute orientation using conjugate points is a well known procedure. However, to the best of the authors' knowledge, there is no established procedure for estimating the 3-D similarity transformation parameters while using corresponding linear features represented by their end points, which might not be conjugate. A newly developed procedure will be explained in the following paragraphs.

Referring to Figure 9, the two points describing the photogrammetric line segment (12) will undergo a 3-D similarity transformation onto the corresponding LIDAR line segment (AB). As it was mentioned earlier, points 1, 2, A, and B need not be conjugate. The objective here is to introduce the necessary constraints to describe the fact that the model segment (12) coincides with the object segment (AB) after applying the transformation. The coincidence of the photogrammetric points (1 and 2) with the LIDAR segment (AB), after applying the transformation

function, can be mathematically described by Equations 3 and 4, respectively.

$$\begin{bmatrix} X_T \\ Y_T \\ Z_T \end{bmatrix} + S\ R_{(\Omega,\ \Phi,\ K)} \begin{bmatrix} X_1 \\ Y_1 \\ Z_1 \end{bmatrix} = \begin{bmatrix} X_A \\ Y_A \\ Z_A \end{bmatrix} + \lambda_1 \begin{bmatrix} X_B - X_A \\ Y_B - Y_A \\ Z_B - Z_A \end{bmatrix} \quad (3)$$

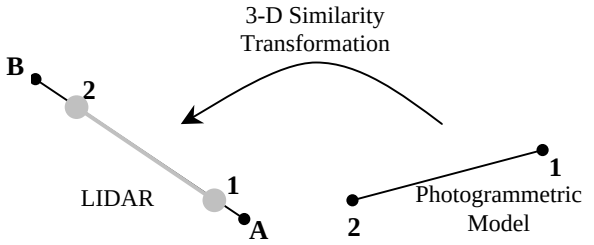

Figure 9. - The similarity measure between photogrammetric and LIDAR linear features

$$\begin{bmatrix} X_T \\ Y_T \\ Z_T \end{bmatrix} + S\ R_{(\Omega,\ \Phi,\ K)} \begin{bmatrix} X_2 \\ Y_2 \\ Z_2 \end{bmatrix} = \begin{bmatrix} X_A \\ Y_A \\ Z_A \end{bmatrix} + \lambda_2 \begin{bmatrix} X_B - X_A \\ Y_B - Y_A \\ Z_B - Z_A \end{bmatrix} \quad (4)$$

Where $(X_T\ Y_T\ Z_T)^T$, in the above equations, is the translation vector between the origins of the photogrammetric and LIDAR coordinate systems, R is the 3-D rotation matrix between the LIDAR and photogrammetric coordinate systems, and (S, λ_1, and λ_2) are scale factors. Subtracting Equation 4 from 3 yields Equation 5.

$$(\lambda_2 - \lambda_1) \begin{bmatrix} X_B - X_A \\ Y_B - Y_A \\ Z_B - Z_A \end{bmatrix} = S\ R_{(\Omega,\ \Phi,\ K)} \begin{bmatrix} X_2 - X_1 \\ Y_2 - Y_1 \\ Z_2 - Z_1 \end{bmatrix} \quad (5)$$

Combining the scale factors (S, λ_1, and λ_2) in Equation 5 into a single scale factor (λ) leads to Equation 6.

$$\begin{bmatrix} X_B - X_A \\ Y_B - Y_A \\ Z_B - Z_A \end{bmatrix} = \lambda\ R_{(\Omega,\ \Phi,\ K)} \begin{bmatrix} X_2 - X_1 \\ Y_2 - Y_1 \\ Z_2 - Z_1 \end{bmatrix} \quad (6)$$

Equation 6 emphasizes the concept that photogrammetric line segments should be parallel to conjugate LIDAR line segments after applying the rotation matrix. To recover the elements of the rotation matrix, Equation 6 is further manipulated and rearranged by dividing the first and second rows by the third one to eliminate λ resulting in Equations 7.

$$\begin{aligned} \frac{(X_B - X_A)}{(Z_B - Z_A)} &= \frac{R_{11}(X_2 - X_1) + R_{12}(Y_2 - Y_1) + R_{13}(Z_2 - Z_1)}{R_{31}(X_2 - X_1) + R_{32}(Y_2 - Y_1) + R_{33}(Z_2 - Z_1)} \\ \frac{(Y_B - Y_A)}{(Z_B - Z_A)} &= \frac{R_{21}(X_2 - X_1) + R_{22}(Y_2 - Y_1) + R_{23}(Z_2 - Z_1)}{R_{31}(X_2 - X_1) + R_{32}(Y_2 - Y_1) + R_{33}(Z_2 - Z_1)} \end{aligned} \quad (7)$$

A pair of conjugate line segments yields two equations, which contribute towards the estimation of two rotation angles, the azimuth and pitch, along the line. On the other hand, the roll angle across the line cannot be estimated, refer to Figure 10a. Hence a minimum of two non-parallel lines is needed to recover the three elements of the rotation matrix (Ω, Φ, K), Figure 10b.

Now, one needs to investigate how to recover the scale factor and the shift components. We start by rewriting Equation 3 for the first point along the photogrammetric line (1) in the form in Equation 8, which can be rearranged to produce Equation 9. The scale factor λ_1 in Equation 9 can be eliminated by dividing the first and second rows by the third one producing Equations 10.

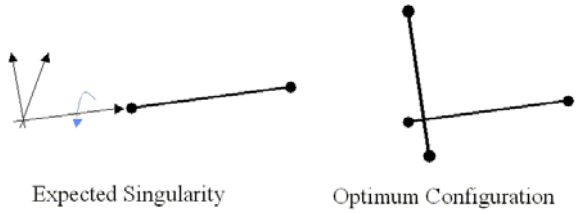

Figure 10. - Singular (a) and optimum (b) configurations to recover rotation angles

$$\begin{bmatrix} X_T \\ Y_T \\ Z_T \end{bmatrix} + S \begin{bmatrix} x_1 \\ y_1 \\ z_1 \end{bmatrix} = \begin{bmatrix} X_A \\ Y_A \\ Z_A \end{bmatrix} + \lambda_1 \begin{bmatrix} X_B - X_A \\ Y_B - Y_A \\ Z_B - Z_A \end{bmatrix} \quad (8)$$

where,

$$\begin{bmatrix} x_1 & y_1 & z_1 \end{bmatrix}^T = R_{(\Omega,\ \Phi,\ K)} \begin{bmatrix} X_1 & Y_1 & Z_1 \end{bmatrix}^T$$

$$\lambda_1 \begin{bmatrix} X_B - X_A \\ Y_B - Y_A \\ Z_B - Z_A \end{bmatrix} = \begin{bmatrix} X_T + S\ x_1 - X_A \\ Y_T + S\ y_1 - Y_A \\ Z_T + S\ z_1 - Z_A \end{bmatrix} \quad (9)$$

$$\begin{aligned} \frac{(X_B - X_A)}{(Z_B - Z_A)} &= \frac{(X_T + S\ x_1 - X_A)}{(Z_T + S\ z_1 - Z_A)} \\ \frac{(Y_B - Y_A)}{(Z_B - Z_A)} &= \frac{(Y_T + S\ y_1 - Y_A)}{(Z_T + S\ z_1 - Z_A)} \end{aligned} \quad (10)$$

Similar to Equations 10, Equations 11 can be written for the second point along the photogrammetric line (2). Finally, Equations 10 and 11 can be reduced to the two independent constraints in Equations 12.

$$\begin{aligned} \frac{(X_B - X_A)}{(Z_B - Z_A)} &= \frac{(X_T + S\ x_2 - X_A)}{(Z_T + S\ z_2 - Z_A)} \\ \frac{(Y_B - Y_A)}{(Z_B - Z_A)} &= \frac{(Y_T + S\ y_2 - Y_A)}{(Z_T + S\ z_2 - Z_A)} \end{aligned} \quad (11)$$

$$\frac{(X_T + S\ x_1 - X_A)}{(Z_T + S\ z_1 - Z_A)} = \frac{(X_T + S\ x_2 - X_A)}{(Z_T + S\ z_2 - Z_A)}$$
$$\frac{(Y_T + S\ y_1 - Y_A)}{(Z_T + S\ z_1 - Z_A)} = \frac{(Y_T + S\ y_2 - Y_A)}{(Z_T + S\ z_2 - Z_A)} \quad (12)$$

A pair of conjugate line segments produces two constraints of the form in Equations 12, which contribute towards the estimation of two parameters. Two pairs of intersecting line segments yield four equations. The shift components can be estimated (using the intersection points). However, the scale factor cannot be recovered, Figure 11a. Therefore, at least two non-coplanar line segments are needed to recover these parameters, Figure 11b. In summary, a minimum of two non-coplanar line segments is needed to recover the seven elements of the 3-D similarity transformation. It is important to note that at this stage the correspondence between linear features in photogrammetric and LIDAR data is established manually. Automatic identification of conjugate line segments will be the focus of future research.

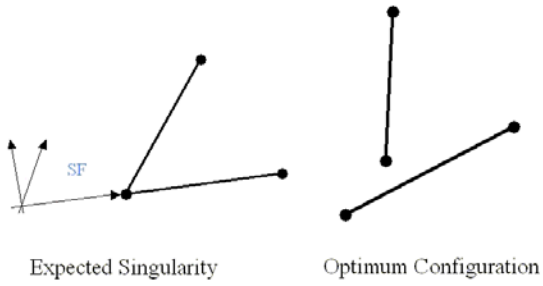

(a) (b)

Figure 11. - Singular (a) and optimum (b) configurations to recover the scale and shift components

So far, we have the addressed the three basic components of the registration methodology. First, straight line segments are chosen as the registration primitives. Second, a 3-D similarity transformation is utilized as the registration transformation function. This transformation assumes the absence of any biases, which cannot be modeled by rigid-body transformation, in the involved photogrammetric and LIDAR systems. Third, the similarity measure is formulated based on the selected primitives, transformation function, and processing methodology. The performance of these components will be evaluated in the experimental result section using real data that have been captured by a professional analog camera, an amateur digital camera, and a high end LIDAR system.

3. EXPERIMENTAL RESULTS

3.1 Objectives

The experiments are designed to address the following issues:

1. The feasibility of using straight-line segments for the co-registration of LIDAR and photogrammetric data.
2. Comparative analysis of the performance of different extraction approaches of linear features from the LIDAR data. The first approach utilizes the raw LIDAR data for plane fitting followed by an intersection procedure. The second approach uses interpolated range and intensity images for an easier identification of the LIDAR linear features.
3. Comparative analysis of the influence of different interpolation techniques on the quality of the extracted linear features from the intensity and range images.
4. Comparative analysis of different processing methodologies. The first methodology is based on direct incorporation of the LIDAR linear features in the photogrammetric triangulation. The second methodology, utilizes independently derived photogrammetric and LIDAR linear features to solve the absolute orientation problem.
5. Comparative analysis of the performance of professional analog and amateur digital cameras.

Within the conducted experiments, the performance will be judged by the quality of fit between conjugate features after the registration procedure and/or check point analysis.

3.2 Involved datasets and processing schemes

Two photogrammetric datasets and one LIDAR dataset are involved in this study. Table 1 summarizes the properties of the photogrammetric datasets (scanned analog images captured by a professional analog camera – RC-10 and digital images captured by an amateur digital camera – SONY-F717). The table also shows expected horizontal and vertical accuracy from each dataset considering the pixel size, image coordinate measurement accuracy, image scale, and height-base ratio. The LIDAR dataset was captured using an OPTECH ALTM 2050 laser scanner with an average flying height of 975m and mean point density of 2.24 points/m^2 (~0.7m point spacing). The range and intensity data were recorded. According to the sensor and flight specifications, 0.5m horizontal and 0.15m vertical accuracies are expected.

TABLE 1: SPECIFICATIONS OF THE PHOTOGRAMMETRIC DATASETS

Camera type & model	RC-10 analog	SONY-F717 digital
Focal length (mm)	153.167	11.6761
# of images	6	17
# of control points	54	31
Avg. flying height (m)	975	737
Avg. base (m)	540	221
Pixel size (mm)	0.024	0.004
Image measurement accuracy (mm)	± 0.024	± 0.004
Expected accuracy (assuming one pixel measurement error)		
planimetric (m)	0.15	0.25
vertical (m)	0.39	1.19

Tie and control points as well as linear features are measured in the image blocks. These measurements are incorporated in several bundle adjustment experiments. The datum of the photogrammetric model has been established by using either control points, which have been collected by geodetic measurements, or control lines from the LIDAR data. The outcome from the bundle adjustment includes the EOP of the involved imagery, the ground coordinates of the tie points, and the ground coordinates of the end points defining the tie lines. In the mean time, LIDAR features have been extracted using two approaches. The first approach utilizes the raw range data to identify neighboring planar patches, which are then intersected. The second approach manipulates interpolated range and intensity images to identify the corresponding linear features. For the second approach, two sets of range and intensity images are generated from the raw LIDAR points using two interpolation schemes, which will be denoted I_1 and I_2, respectively. I_1 is based on a pixel size of 0.3m and 4m-radius search window while using 2nd degree inverse distance weighting. On the other hand, I_2 is based on 1.0m pixel size using the nearest neighbor interpolation technique.

3.3 Direct incorporation of LIDAR linear features as control in photogrammetric triangulation

In those experiments, extracted linear features from the interpolated intensity and range imagery are used as the source of control for the photogrammetric model. Due to limitations in identifying a sufficient number of neighboring planar patches over the entire area, linear features from patch intersection are not enough for establishing a proper datum for the photogrammetric adjustment. However, extracted LIDAR lines from patch intersection will be utilized in the analysis in section 3.4.

3.3.1 LIDAR/RC-10

Extracted straight-line segments from the interpolated LIDAR datasets (I_1 and I_2) are used in separate experiments as the source of control for the photogrammetric triangulation of the RC-10 image block. Table 2 summarizes the quality of the aligned photogrammetric model through check point analysis. More specifically, the photogrammetric coordinates of the check points are compared with these derived from independent geodetic measurements. The comparison results in Table 2 include the average difference between the photogrammetric and geodetic coordinates together with the corresponding standard deviation.

3.3.2 LIDAR/SONY-F717

Similar to the previous experiments, extracted straight-line segments from the two LIDAR datasets (I_1 and I_2) are used in separate experiments as the source of control information for the photogrammetric triangulation of the SONY-F717 image block. Table 3 summarizes the quality of the aligned photogrammetric model through check point analysis.

Comparing the results in Tables 2 and 3, one can observe the following:

1. Based on the standard deviations associated with the check points, the RC-10 data is showing better alignment when compared to the SONY data. This should come as no surprise since the expected accuracy from the RC-10 is superior to that from the SONY (refer to Table 1).
2. Based on the standard deviations associated with the check points, the RC-10 is showing a better alignment when using linear features from the I_2 dataset in place of these derived from I_1. This is expected since the point spacing in I_2 (1.0m) is closer to the point spacing associated with the raw LIDAR points (0.7m). In other words, I_2 is a more realistic sampling considering the raw point density. Thus, the interpolation point density should be selected to be commensurate with the raw LIDAR data.
3. Based on the standard deviations associated with the check points, the SONY data is showing almost identical alignment quality when using LIDAR features derived from the I_1 and I_2 datasets. This is expected since the photogrammetric errors for the SONY block (Table 1) are more dominant than the errors in the derived LIDAR linear features using different interpolation techniques.
4. Comparing the mean and the corresponding standard deviations from the check point analysis, especially for the RC-10 dataset, one can identify a persistent bias in the X and Z directions (i.e., the mean value is significantly larger than the standard deviation). The origin of this bias will be elaborated on in a later discussion.

TABLE 2: CHECK POINT ANALYSIS FOR LIDAR/RC-10 DATASETS

	LIDAR set I_1	LIDAR set I_2
# of control lines	80	79
# of check points	32	32
ΔX (m)	0.75 (±0.51)	0.65 (±0.28)
ΔY (m)	-0.10 (±0.43)	-0.15 (±0.26)
ΔZ (m)	-0.75 (±0.36)	-0.69 (±0.42)

TABLE 3: CHECK POINT ANALYSIS FOR LIDAR/SONY-F717 DATASETS

	LIDAR set I_1	LIDAR set I_2
# of control lines	68	68
# of check points	31	31
ΔX (m)	0.38 (±0.63)	0.42 (±0.70)
ΔY (m)	0.35 (±0.70)	0.20 (±0.67)
ΔZ (m)	-0.49 (±1.11)	-0.51 (±1.12)

3.4 LIDAR lines for the absolute orientation of the photogrammetric model

In these experiments, separate photogrammetric models involving tie linear features have been generated from the RC-10 and SONY image blocks. The datum for these models is established using the coordinates of precisely surveyed ground control points. The object points defining the involved tie line segments are derived from the photogrammetric bundle adjustment. These segments together with the corresponding LIDAR features are used in an absolute orientation procedure. The LIDAR features are either derived from the interpolated I_1 and I_2 datasets or plane fitting and intersection procedures. Assuming that the LIDAR data and the control points share the same reference frame, one would expect the parameters of the 3-D similarity transformation to be as follows: ($X_T = Y_T = Z_T = 0.0$m, $\Omega = \Phi = K = 0.0°$, and $S = 1.0$). Therefore, significant deviations from these optimum values indicate the presence of biases between the control points and LIDAR reference frames.

3.4.1 LIDAR/RC-10

Table 4 lists the parameters of the absolute orientation relating the LIDAR lines and the RC-10 lines, which have been derived from I_1, I_2, and patch intersection, respectively. The average normal vector components between conjugate photogrammetric and LIDAR lines before and after the absolute orientation are shown in Table 5. A closer investigation of Tables 4 and 5 reveal the following facts:

1. Regardless of the origin of the utilized LIDAR linear features, one can observe a persistent bias in the X and Z directions between the reference frames associated with the LIDAR model and control points (refer to Table 4). This is compatible with the reported bias values in section 3.3. After thorough investigation, it was found that the available control points are given relative to the SAD 69 reference frame prior to 1998. On the other hand, LIDAR data was based on the SAD 69 after the 1998's adjustment. Certain biases, especially in the *X* direction, have been reported between the two versions. In addition, half a meter bias has been detected in the LIDAR data in the *Z* direction.
2. The standard deviations of the normal distances between the LIDAR and photogrammetric lines before and after the absolute orientation (Table 5) indicate that the best fit is achieved for the linear features, which have been derived from patch intersection followed by these from I_2 and I_1. This is not surprising since it is expected that the patch intersection will lead to the highest quality linear features (they are based on the raw LIDAR data). However, the quality of these features will manifest itself only if the photogrammetric linear features are of commensurate or better quality. Therefore, one should expect better fit when working with the RC-10 data. On the other hand, one should not expect better performance when working with the SONY data, where the photogrammetric features are only compatible with these derived from the I_1 dataset (refer to the analysis in 3.3.2).
3. The standard deviations in Table 4 associated with the estimated transformation parameters derived from the linear features produced by the patch intersection show slightly less quality when compared to these derived from I_1 and I_2. This lower quality is only due to the low redundancy resulting from having fewer features (twenty-three versus eighty and seventy-nine line segments).
4. The average values of the normal distances between the photogrammetric and LIDAR lines after the absolute orientation (Table 5) indicate the success of the registration procedure in removing the biases between the respective reference frames.

TABLE 4: 3-D SIMILARITY PARAMETERS BETWEEN LIDAR AND RC-10 MODELS

	I_1		I_2		Patch intersection	
# of lines	80		79		23	
Scale	0.999526	±0.00033	1.000097	±0.00025	1.000050	±0.00038
X_T (m)	0.62	±0.14	0.56	±0.11	0.53	±0.15
Y_T (m)	0.19	±0.15	0.04	±0.11	-0.11	±0.14
Z_T (m)	-0.98	±0.07	-1.07	±0.05	-0.86	±0.08
Ω (°)	-0.003	±0.014	-0.004	±0.010	0.029	±0.029
Φ (°)	0.030	±0.012	0.029	±0.009	0.083	±0.017
K (°)	-0.020	±0.018	0.009	±0.013	-0.023	±0.021

TABLE 5: OVERALL NORMAL VECTOR BETWEEN CONJUGATE PHOTOGRAMMETRIC (RC-10) AND LIDAR LINES BEFORE AND AFTER ABSOLUTE ORIENTATION

	I_1		I_2		Patch intersection	
Before absolute orientation						
DX (m)	-0.26	±1.00	-0.24	±0.54	-0.23	±0.25
DY (m)	-0.15	±1.09	-0.01	±0.56	0.02	±0.20
DZ (m)	0.96	±0.64	1.01	±0.65	0.72	±0.37
After absolute orientation						
DX (m)	0.03	±0.96	0.04	±0.52	0.005	±0.13
DY (m)	-0.03	±1.04	0.02	±0.54	-0.057	±0.12
DZ (m)	-0.02	±0.45	-0.06	±0.46	-0.115	±0.41

3.4.2 LIDAR/SONY-F717

Table 6 lists the parameters of the absolute orientation relating the LIDAR lines and the SONY-F717 lines, which have been derived from the I_1 and I_2 datasets. The average normal vector components between conjugate photogrammetric and LIDAR lines before and after the absolute orientation are shown in Table 7. A closer investigation of Tables 6 and 7 reveal

the following facts:

1. Referring to Table 6, one can observe the previously reported biases between the photogrammetric and LIDAR models. As it was mentioned earlier, this is compatible with the biases between the reference frames associated with the LIDAR and control points.
2. The average values of the normal distances between the photogrammetric and LIDAR lines after the absolute orientation (Table 7) indicate the success of the registration procedure in removing the biases between the respective reference frames.
3. Referring to Table 7, one can observe a slight improvement in the quality of fit (slightly lower standard deviations) between the photogrammetric model and the derived LIDAR features from I_2 when compared to these derived from I_1. However, this improvement is not as significant as that associated with the RC-10 data. This is expected since the photogrammetric errors in the SONY data are more dominant than these arising from using different interpolation techniques.

TABLE 6: 3-D SIMILARITY PARAMETERS BETWEEN LIDAR AND SONY MODELS

	I_1		I_2	
# of lines	68		68	
Scale	0.999407	±0.0005	1.00015	±0.0006
X_T (m)	0.70	±0.19	0.69	±0.20
Y_T (m)	-0.09	±0.19	-0.08	±0.2
Z_T (m)	-0.63	±0.13	-0.69	±0.1
Ω (°)	-0.083	±0.037	-0.05	±0.027
Φ (°)	0.0005	±0.036	0.012	±0.026
K (°)	0.131	±0.039	0.076	±0.041

TABLE 7: OVERALL NORMAL VECTOR BETWEEN CONJUGATE PHOTOGRAMMETRIC (SONY F717) AND LIDAR LINES BEFORE AND AFTER ABSOLUTE ORIENTATION

	I_1		I_2	
Before absolute orientation				
DX (m)	-0.29	±1.08	-0.33	±0.69
DY (m)	-0.02	±1.08	0.05	±0.60
DZ (m)	-0.52	±1.20	-0.57	±1.17
After absolute orientation				
DX (m)	0.08	±1.03	0.03	±0.60
DY (m)	-0.07	±1.09	0.02	±0.59
DZ (m)	-0.11	±1.16	-0.12	±1.14

4. CONCLUSIONS AND FUTURE WORK

This paper presented a comprehensive registration methodology for the alignment of LIDAR and photogrammetric models relative to a common reference frame using straight-line features. The straight-line segments have been chosen as the registration primitives since they can be reliably extracted from the photogrammetric and LIDAR data. A 3-D similarity transformation has been selected as the transformation function relating the datasets in question. This transformation assumes the absence of biases, which cannot be modeled by rigid-body transformation, between the LIDAR and photogrammetric datasets. Also, appropriate similarity measures have been introduced to ensure the coincidence of the photogrammetric and LIDAR features after applying the registration transformation function. The similarity measure can be implemented in two different ways. The first alternative directly incorporates the LIDAR features as a source of control in the photogrammetric bundle adjustment. The second alternative starts by independent processing the LIDAR and photogrammetric data. In this case, the photogrammetric model can be established by selecting an arbitrary datum. Afterwards, conjugate photogrammetric and LIDAR features are utilized to derive the parameters of the absolute orientation relating the photogrammetric and LIDAR reference frames. In addition to the registration methodologies, we presented two techniques for the extraction of linear features from LIDAR data. The first technique utilized the raw LIDAR data to identify neighboring planar patches, which are then intersected to produce the linear features. The second technique, utilized interpolated intensity and range images for an easier extraction of the linear features.

To test the feasibility of the developed methodologies, we conducted several experiments using real data captured by an analog professional camera (RC-10), an amateur digital camera (SONY-F717), and a high end LIDAR system (OPTECH ALTM 2050). The outcome from these experiments suggests the following:

- Straight line features proved its suitability in establishing a common reference frame for the LIDAR and photogrammetric surfaces.
- The quality of the LIDAR and photogrammetric features plays an important role in the quality of the final fit between the respective models. In this regard, the following has been observed:
  - Linear features from the RC-10 data exhibit higher quality when compared to these derived from the SONY-F717 data. This should be expected due to the better height-base ratio associated with the RC-10 image block.
  - LIDAR linear features, which are derived from neighboring patch intersection, are more accurate than these derived from the interpolated intensity and range images.
  - Derived LIDAR linear features from the interpolated range and intensity images show better quality if the sampling interval of the produced imagery is commensurate with the point density of the raw LIDAR data.
  - The quality of the derived LIDAR linear features influences the quality of the registration if the photogrammetric features exhibit a commensurate or better quality.

- The registration methodology is capable of identifying biases and systematic errors between the involved datasets. The quality of fit between the registered models is improved following the removal of these biases.
- Direct incorporation of the LIDAR features in the photogrammetric triangulation is equivalent to independent processing of the image and LIDAR data followed by absolute orientation. In other words, these processing methodologies will not affect the quality of the registration outcome. The only advantage of the latter methodology is the possibility of investigating the discrepancy pattern between the photogrammetric and LIDAR models after the absolute orientation. Such investigation might give meaningful clues about these discrepancies, which could be linked to systematic biases in the involved systems. On the other hand, the presence of systematic errors while directly using the LIDAR features in the triangulation will manifest itself in higher residuals. The investigation of the residual pattern and relating it to systematic errors is not a trivial task.

Future research work will focus on checking the quality of fit between the registered models to identify the presence of systematic errors in either system. In this regard, the discrepancy pattern between the aligned models might give some clues about the nature of existing biases and/or mis-calibrated system components. In addition, we will address the automation of the extraction of linear features from photogrammetric and LIDAR data together with the correspondence between conjugate features. Also, we will be looking at the possibility of developing new visualization tools for an easier portrayal of the registration outcome. Superposition of the derived ortho-photos and LIDAR data, Figure 12, can be used to check the quality of the registration process as well as showing the different characteristics of the involved datasets. Finally, registered multi-temporal datasets will be inspected for the possibility of developing automatic change detection techniques. For example, Figure 13 shows the presence of object space changes between the ortho-photos derived from RC-10 and SONY-F717 imagery, which have been captured at different epochs.

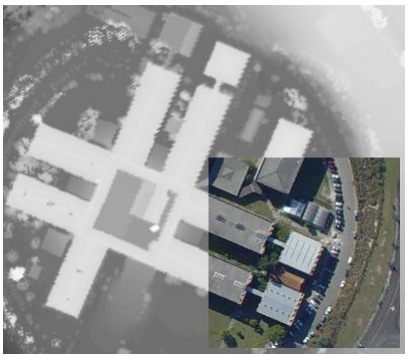

Figure 12. - A part of a LIDAR intensity image is overlaid by a patch from the SONY-F717 ortho-photo.

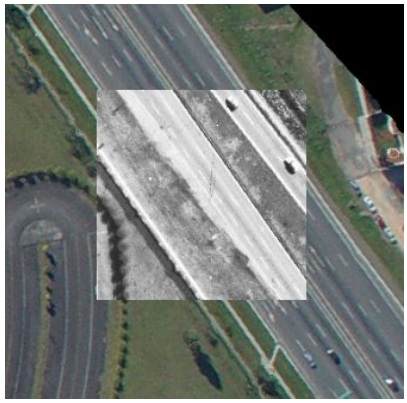

Figure 13. - Observed changes between the RC-10 (foreground) and SONY-F717 (background) ortho-photos (Note that the road has been widened in the SONY ortho-photo).

ACKNOWLEDGMENT

We would like to thank the GEOIDE (GEOmatics for Informed Decisions) Network of Centers of Excellence of Canada for their financial support of this research. The authors are also indebted to the Technology Institute for Development – LACTEC – UFPR, for providing the LIDAR data.

REFERENCES

BALTSAVIAS, E., 1999. A comparison between photogrammetry and laser scanning. **ISPRS Journal of Photogrammetry & Remote Sensing**, 54(1):83–94.

BROWN, L., 1992. A survey of image registration techniques, **ACM Computing Surveys** 24(4): 325-376.

HABIB, A., T. Schenk, 1999. New approach for matching surfaces from laser scanners and optical sensors, **The International Archives of Photogrammetry and Remote Sensing and Spatial Information Sciences**, 32(3W14):55-61.

HABIB, A., Y. Lee, and M. Morgan, 2001. Surface matching and change detection using the modified Hough transform for robust parameter estimation. **Photogrammetric Record Journal,** 17(98): 303-315.

HABIB, A., Y. Lee, M. Morgan, 2002a. Bundle adjustment with self-calibration using straight lines. **Photogrammetric Record Journal,** 17(100): 635-650.

HABIB, A., S. Shin, M. Morgan, 2002b. *New approach for calibrating off-the-shelf digital cameras*. In **ISPRS Commission III Symposium**

"Photogrammetric Computer Vision", Graz, Austria, September 9 – 13, 2002.

EBNER, H., and T. Ohlhof, 1994. Utilization of ground control points for image orientation without point identification in image space. In **The International Archives of Photogrammetry and Remote Sensing and Spatial Information Sciences**, 30(3/1):206–211.

KILIAN, J., N. Haala, and M. Englich, 1996. Capture and evaluation of airborne laser scanner data. In **The International Archives of Photogrammetry and Remote Sensing and Spatial Information Sciences**, 31(B3):383-388.

POSTOLOV, Y., A. Krupnik, and K. McIntosh, 1999. Registration of airborne laser data to surfaces generated by photogrammetric means. In **The International Archives of Photogrammetry and Remote Sensing and Spatial Information Sciences**, 32(3W14):95-99.

SCHENK, T., and B. Csathó, 2002. Fusion of LIDAR data and aerial imagery for a more complete surface description. In **The International Archives of Photogrammetry and Remote Sensing and Spatial Information Sciences**, 34(3A):310-317.

Invited Paper